

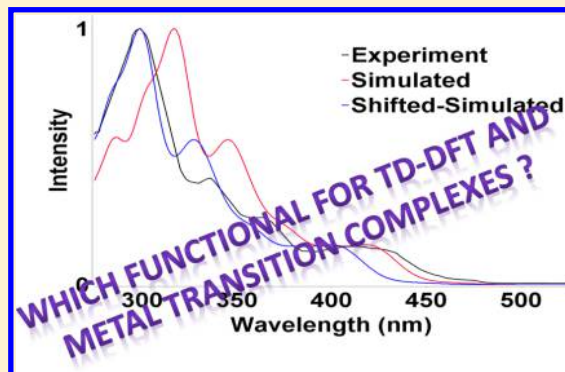
TD-DFT Benchmark on Inorganic Pt(II) and Ir(III) Complexes

Camille Latouche, Dimitrios Skouteris, Federico Palazzetti, and Vincenzo Barone*

Scuola Normale Superiore, Piazza dei Cavalieri 7, 56126 Pisa, Italy

S Supporting Information

ABSTRACT: We report in the present paper a comprehensive investigation of representative Pt(II) and Ir(III) complexes with special reference to their one-photon absorption spectra employing methods rooted in density functional theory and its time dependent extension. We have compared nine different functionals ranging from generalized gradient approximation (GGA) to global or range-separated hybrids, and two different basis sets, including pseudopotentials for 4 iridium and 7 platinum complexes. It turns out that hybrid functionals with the same exchange part give comparable results irrespective of the specific correlation functional (i.e., B3LYP is very close to B3PW91 and PBE0 is very close to MPW1PW91). More recent functionals, such as CAM-B3LYP and M06-2X, overestimate excitation energies, whereas local functionals (BP86 -GGA-, M06-L -Meta GGA-) strongly underestimate transition energies with respect to experimental results. As expected, basis set effects are weak, and the use of a triple- ζ polarized (def2-TZVP) basis set does not significantly improve the computed excitation energies with respect to a classical double- ζ basis set (LANL2DZ) augmented by polarization functions, but it significantly raises the computational effort.



■ INTRODUCTION

In the past decade, methods rooted in the density functional theory (DFT) and its time dependent extension (TD-DFT) have become widespread tools used by theoretically and experimentally oriented chemists to understand, rationalize, and predict the optical behavior of compounds ranging from small organic molecules to large complex dyes and biomolecule building blocks. This success of TD-DFT has arisen from the remarkable accuracy/computational-time ratio allowing also nonspecialists to perform fast calculations and obtain reasonable results, which could be directly compared to experimental data. Furthermore, ongoing developments are pushing this computational tool beyond its original barriers.

For organic molecules, and especially dyes, one may quote the extensive benchmarks performed by Jacquemin et al. over the last few years, showing how TD-DFT can provide accurate results for such types of compounds after inclusion of some specific corrections (especially accounting for solvent effects).^{1–14} However, despite the increasing use of the same approach for metal complexes,^{15–26} or in metal cluster chemistry,^{27–30} benchmarks for those compounds remain difficult to perform, especially due to the requested resources. In any case, some preliminary benchmark studies have provided encouraging results.^{31–35} Furthermore, most vertical electronic transitions of organic molecules are of $\pi-\pi^*$ or $n-\pi^*$ type, whereas for metal complexes, the metal d orbitals are often involved, leading to the so-called metal-to-ligand charge transfer (MLCT). Among the different inorganic metal complexes and organometallics, absorption spectra of platinum and iridium derivatives are often dominated by ¹MLCT/³MLCT transitions, which also play a significant role in possible

technological applications (e.g., NLO, luminescence).^{36–48}

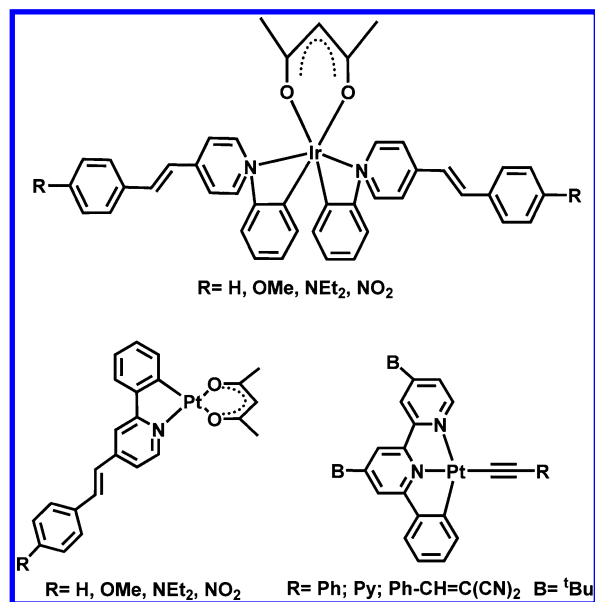
These considerations prompted us to start a comprehensive investigation with the aim of obtaining further insights into the spectroscopic behavior of such compounds and of proposing reliable computational protocols, which could also profitably be used for other transition metal compounds. We have compared different functionals and basis sets trying to define the methods of choice by comparison to experimental results reported in previous investigations. The targeted complexes are of medium-large size but, due to the large number of electrons, we have chosen only three types of backbones, two for Pt(II) and one for Ir(III). Moreover, despite the quite limited number of studied complexes (11), they already represent a quite extensive benchmark involving ~500 computations. In the cases of the iridium and one of the platinum backbones, the R substituents are the same, thus permitting a direct correlation between the accuracy of the computed excitation energies and the drawing/withdrawing character of the substituent (Scheme 1).

■ COMPUTATIONAL DETAILS

All calculations have been carried out with a locally modified version of the Gaussian suite of programs.⁵² All the data postprocessing has been performed by the VMS-draw graphical user interface.⁵³ To perform this benchmark, we have employed two conventional functionals based on the generalized gradient approximation (GGA), namely BP86^{54,55} and Meta-GGA M06-L,⁵⁶ the hybrids B3LYP,^{57–59} B3PW91,^{55,57,60}

Received: March 18, 2015

Published: June 9, 2015

Scheme 1. Set of Investigated Complexes^{46–51}

MPW1PW91,^{60–62} PBE0,^{63,64} M06 and its derivative M06-2X,⁶⁵ and the long-range corrected CAM-B3LYP⁶⁶ functional. They have been associated with two basis sets, LANL2DZ^{67–70} augmented by polarization functions, and def2-TZVP.⁷¹ Bulk solvent effects have been taken into account by means of the polarizable continuum model (PCM) in the linear response (LR) approximation.^{72–74} In the case of Pt-acac, we used DMF as solvent, whereas for other complexes, we retain the same solvent used in the corresponding experiments. Starting from geometries optimized for the ground electronic state, single point TD-DFT computations have been performed to obtain the vertical electronic transition energies. In some cases, analytical gradients of excited state energies have been computed at these geometries to allow evaluation of vibronic effects by our general time dependent implementation employing the vertical gradient (VG) approximation.^{52,53,75} In this model, the frequencies and normal modes of the excited state are taken to be equal to those of the ground state, and the shift between the minima of the two states is estimated by the gradient of the excited state at the geometry of the ground state.

RESULTS AND DISCUSSION

As mentioned above, we have investigated transition wavelengths and oscillator strengths for all of the compounds using two different basis sets and, for each of them, nine density functionals. The functionals can be grouped into sets providing very similar trends for all compounds. Thus, the B3LYP and B3PW91 functionals give similar results, and the same is true for the PBE0 and MPW1PW91 functionals (and, to a lesser extent, for the M06 functional). Finally, M06-2X and CAM-B3LYP also give very similar transition wavelengths. The two remaining local functionals, BP86 and M06-L, give unique results, which are not easily comparable to those of the other functionals.

For ease of description, we will refer to B3LYP and B3PW91 as the B3 group, PBE0, MPW1PW91, and M06 as the PBE-M06 group, M06-2X and CAM-B3LYP as the CCT group, and to BP86 and M06-L as the BP86/M06-L group of functionals.

We start the discussion from the four derivatives of the Pt(II)-acac complex for which extensive experimental data are available.⁴⁹

Pt(II) complexes with R = H, OMe, NEt₂, and NO₂. 1. *R* = *H*. Using the LANL2DZ basis set, the three strongest transitions predicted by the B3 group are found around 405, 350, and 338 nm (oscillator strengths of 0.71, 0.55, and 0.18, respectively). Using the def2-TZVP basis set, the corresponding transitions lie at 404, 345, and 331 nm. The first transition correlates well with the experimental transition of 392 nm, whereas the second and third ones fall at rather longer wavelengths than the experimental values of 316 and 248 nm. The corresponding transitions predicted by the PBE-M06 group fall at 390, 337, and 322 nm for the LANL2DZ basis set and at 387, 332, and 322 nm for the def2-TZVP set. Overall, the PBE-M06 group therefore performs better than the B3 one, the first transition falling exactly on the experimental one and the second being substantially closer. On the other hand, the third transition is still quite far from the experimental value. We also stress that a small transition appears lower in energy around 440 nm for the B3 group, whereas it is blue-shifted by 20 nm for the PBE-M06 functionals. The CCT group with both basis sets gives a very strong transition around 335 nm, accompanied by weaker transitions at 340 (M06-2X) to 350 (CAM-B3LYP) nm and 286 (M06-2X) to 291 (CAM-B3LYP) nm.

The BP86 functional gives generally too high wavelengths (515, 429, and 409 nm in the LANL2DZ basis set and 514, 423, and 405 nm in def2-TZVP), which are not at all immediately comparable with the experimental values. The same is true for the M06-L functional (477, 393, and 374 nm in LANL2DZ and 479, 387, and 372 nm in def2-TZVP), albeit to a much lesser extent.

2. *R* = *OMe*. Regarding this substituent within the LANL2DZ basis set, the B3 group predicts a moderately strong transition at 432 nm, a strong one at 416 nm, and again two moderate ones at 363 and 336 nm (oscillator strengths of 0.20, 1.00, 0.21, and 0.19, respectively). The corresponding numbers for the def2-TZVP basis set are 427, 413, 358, and 333 nm. Looking at the experimental bands (386, 336, 289, and 253 nm), it can be seen that the B3 predictions fall substantially lower than the experimental ones. In the case of the PBE-M06 group, the situation is definitely better. The strongest transitions are predicted at 410, 399, 344, and 322 nm for the LANL2DZ basis set. Using the def2-TZVP basis set, one obtains 406, 396, 341, and 319 nm. Even though the predicted lines still fall short of the experimental values, the differences are certainly reduced. The CCT group predicts a very strong transition at 350 nm for LANL2DZ (345 nm for def2-TZVP) with moderate ones at 290, 253, and 240 nm (289, 251, and 237 nm for def2-TZVP). As in the case of *R* = *H*, the BP86 functional gives too high wavelengths (513, 459, 418, and 407 nm in the LANL2DZ basis set and 511, 450, 418, and 405 nm in def2-TZVP). The same is true for the M06-L functional (474, 421, 378, and 357 nm in LANL2DZ and 474, 414, 377, and 366 nm in def2-TZVP), again to a lesser extent.

3. *R* = *NEt₂*. There is only one experimental line with this moiety at 432 nm. The B3 functional group predicts a very strong line at 478 nm in the LANL2DZ basis set (471 nm in the def2-TZVP basis set), which is rather close to the experimental value. The prediction of the PBE-M06 functional group is rather better, falling at 456 nm in the LANL2DZ basis set and at 445–450 nm in the def2-TZVP set. The CCT

prediction falls at too short a wavelength at 388 nm with LANL2DZ and 383 nm with def2-TZVP. Finally, consistent with the previous cases, both the BP86 and the M06-L functional predict too high wavelengths (BP86 predicts 596 nm and M06-L predicts 534 nm in the LANL2DZ basis set with the respective values for def2-TZVP being 585 and 524 nm).

4. $R = \text{NO}_2$. There are two experimental lines with $R = \text{NO}_2$ corresponding to 400 and 333 nm. The B3 functional group in the LANL2DZ basis set predicts one very weak transition around 550 nm and two strong lines at around 490 and 405 nm, which are rather lower than the experimental values (oscillator strengths of 0.5 and 0.6, respectively). The corresponding lines predicted by the def2-TZVP basis set fall by 10 nm. As before, the results from the PBE-M06 group are definitely closer to the experimental values, falling at 445 and 378 nm for LANL2DZ basis set and at 440 and 370 nm for the def2-TZVP set (for the two most intense transitions in this spectroscopic region).

Consistently with previous cases, the CCT functional group tends to err on the low side, producing two transitions around 355–348 nm (M06-2X) and 366–357 nm (CAM-B3LYP) for the LANL2DZ basis set. The corresponding lines in the def2-TZVP basis set fall at 352–344 nm (M06-2X) and 362–354 nm (CAM-B3LYP). Moreover, following the previous trend, the BP86 and M06-L functionals tend to overestimate the wavelength with the BP86 predicting transitions at 782 and 530 nm for the LANL2DZ basis set (782 and 521 nm with def2-TZVP) and M06-L giving 708 and 489 nm with the LANL2DZ basis set (693 and 483 nm with def2-TZVP).

Pt(II) Complexes with $R = \text{Ph}$, Py , and $\text{Ph}-\text{CH}=\text{C}(\text{CN})_2$.

1. $R = \text{Ph}-\text{CH}=\text{C}(\text{CN})_2$. The experimental absorption spectrum has been recorded in CH_2Cl_2 , and the following excitation wavelengths were measured: 450, 400, and 330 nm.⁴⁶

For the B3 functionals, a first transition at around 480 nm has been computed but with a very small oscillator strength ($f = 0.0385$). Despite this exception, a very intense transition has been computed around 465, 455, and 445 nm for the B3, M06, and PBE functionals, respectively, together with the LANL2DZ basis set. These values remain almost unchanged when the def2-TZVP basis set is used. CCT functionals overestimate the excitation energies, which have been computed to be around 385 nm with both functionals and independently of the choice of the basis set. Conversely, the GGA and Meta-GGA functionals clearly underestimate the transition energies. For instance, one may quote BP86 to be associated with a very intense transition at 548 nm ($f = 0.9516$). Several weak transitions have been computed for all the classic hybrid functionals in the range of 300–450 nm (except one with a strong oscillator strength around 325 ± 10 nm), which make it difficult to compare their values unambiguously.

2. $R = \text{Ph}$. The experimental absorption of this compound, performed in CH_3CN , gave the following experimental excitation wavelengths: 420, 357, and 330 nm.⁴⁷

B3 functionals computed a first transition around 450 nm with a strong oscillator strength ($f = 0.2379$) using the LANL2DZ basis set. However, when the def2-TZVP basis set was used, the oscillator strength decreased dramatically ($f = 0.0676$). An identical behavior is obtained with PBE's functional but with a computed wavelength closer to the experimental value (430 nm). Surprisingly, the computed transition by the M06 functional exhibited is at ~ 440 nm but with a very weak oscillator strength ($f = 0.0070$). M06-2X and CAM-B3LYP still overestimated the transition energy, and the

opposite behavior is still apparent using local functionals (BP86/M06-L). The recorded absorption value at 357 nm probably corresponds to the computed values at ~ 360 nm for B3 and 345 nm for PBE functionals with a quite strong oscillator strength. Moreover, the strong correction on the first transition with def2-TZVP allows a better description of the other electronic transitions with respect to the experimental values (see the Supporting Information). Finally, the transition around 330 nm is particularly well reproduced by the B3 functionals with transitions around this value, whereas the PBE functional slightly overestimates this energy.

3. $R = \text{Py}$. Transitions were recorded by measuring the absorption in CH_3CN at 420, 360, and 330 nm.⁴⁷ Contrary to $R = \text{Ph}$, the first computed transition has a very weak oscillator strength for all hybrid functionals ($f \approx 0.01$). A transition with oscillator strengths one order of magnitude higher than the previous one is computed for the B3 group at around 400 nm ($f \approx 0.1$) and between 375 and 385 nm for PBE's group. This transition could correspond to the ones computed at 320 and 300 nm for CAM-B3LYP and M06-2X, respectively. As usual, BP86 and M06-L clearly reproduced the experimental data poorly.

Ir(III) Complexes with $R = \text{H}$, OMe , NEt_2 , and NO_2 .

1. $R = \text{H}$. The recorded excitations are at 468, 410, and 370 nm in CH_2Cl_2 solution. If one pays attention to the recorded spectra, the absorbance decreases slowly after 500 nm, suggesting the presence of weak transitions that are not reported by the authors. This information makes it difficult to unambiguously assign the computed excitation with respect to the experimental values. B3 functionals exhibit transitions at approximately 520, 450, 408, and 380 nm with non-negligible oscillator strengths for both basis sets ($f = 0.0701, 0.4185, 0.9237$, and 0.2298 for B3LYP/LANL2DZ, respectively). The computed transitions by PBE's functional are higher in energy than the B3 values. Indeed, the computed excitations are at around 485, 420, 385, and 360 nm ($f = 0.0784, 0.5535, 0.9506$, and 0.2142 using MPW1PW91/def2-TZVP, respectively). M06 shows results between both B3 and PBE's functionals with excitations at 506, 437, 411, and 378 nm in LANL2DZ ($f = 0.0616, 0.5230, 0.8826$, and 0.2336 , respectively). However, one should notice that M06 has been slightly affected by the extension of the basis set. For instance, the computed transition at 506 nm in LANL2DZ shifts to 492 nm with the def2-TZVP basis set, which represents a correction of 14 nm ($\approx 3\%$). The CCT functionals have a net trend to overestimate the excitation energies. For instance, the first computed bright transition is 384 and 373 nm for CAM-B3LYP and M06-2X, respectively, using the LANL2DZ basis set. As for Pt(II) complexes, the GGA and Meta-GGA functionals have difficulties reproducing the excitations due to their net trend to underestimate them.

2. $R = \text{OMe}$. For this complex, the reported experimental transitions are at 475, 415, and 373 nm. One should notice the very small bathochromic effect with respect to the H substituent. However, this trend is not reproduced in our computations, where the first excitations for the B3 group are obtained at approximately 500, 440, 410, and 380 nm ($f = 0.0867, 0.7162, 1.2582$, and 0.2398 , respectively, with B3PW91 together with def2-TZVP). The same trend of results is obtained with the PBE functionals (i.e., the computed transitions are energetically higher than for $R = \text{H}$). For instance, PBE0 together with LANL2DZ gives excitations at 474, 420, 390, and 361 nm. M06 exhibits the same behavior as for the previous compound (i.e., between PBE and the B3

Table 1. Experimental vs Computed Excitation Wavelengths (Oscillator Strength) Using the TD-DFT Method (LANL2DZ+pol)

	experimental	BP86	B3PW91	PBE0	CAM
Ir, R = H ^a	468 (weak)	729 (0.02)	520 (0.07)	486 (0.08)	384 (0.24)
	410 (strong)	630 (0.22)	450 (0.43)	422 (0.58)	344 (1.98)
	370 (strong)		405 (0.93)	384 (1.03)	317 (0.38)
			382 (0.24)	363 (0.24)	
Ir, R = OMe ^a	475 (weak)	693 (0.03)	506 (0.09)	473 (0.12)	381 (0.40)
	415 (strong)	618 (0.24)	445 (0.77)	419 (1.15)	352 (2.53)
	373 (very strong)		410 (1.33)	390 (1.23)	316 (0.23)
			380 (0.28)	346 (0.48)	
Ir, R = NEt ₂ ^a	480 (weak)	688 (0.03)	493 (0.65)	465 (1.31)	391 (3.48)
	433 (strong)	659 (0.12)	472 (2.15)	450 (1.84)	372 (0.13)
	410 (strong)		452 (0.26)	419 (0.07)	
Ir, R = NO ₂ ^a	518 (weak)	1021 (0.22)	676 (0.03)	594 (0.04)	406 (0.24)
	442 (strong)	785 (0.34)	558 (0.39)	499 (0.54)	366 (2.44)
	400 (very strong)	669 (0.06)	482 (0.73)	440 (0.93)	332 (0.41)
			457 (0.14)	420 (0.19)	317 (0.23)
			415 (0.87)	383 (0.99)	
			403 (0.10)	357 (0.10)	
Pt, R = Ph ^b	420 (weak)	602 (0.18)	456 (0.24)	431 (0.24)	348 (0.35)
	357 (strong)	546 (0.02)	389 (0.05)	367 (0.05)	303 (0.19)
	330 (very strong)	515 (0.08)	358 (0.17)	344 (0.21)	293 (0.19)
			332 (0.18)	319 (0.26)	283 (0.50)
			330 (0.09)	312 (0.06)	262 (0.47)
Pt, R = CH=C(CN) ₂ ^c	450 (very strong)	582 (0.09)	482 (0.04)	450 (0.37)	387 (1.67)
	400 (strong)	548 (0.95)	464 (0.49)	445 (1.19)	303 (0.19)
	330 (weak)	542 (0.22)	463 (0.97)	410 (0.02)	285 (0.38)
			434 (0.04)	381 (0.02)	279 (0.19)
			402 (0.03)	331 (0.07)	
			332 (0.24)	319 (0.29)	

^aFrom ref 50. ^bFrom ref 47. ^cFrom ref 46.

group). CAM-B3LYP and M06 also show a decrease of ~5 nm when going from H to OMe adducts.

3. $R = \text{NEt}_2$. The transitions of this adduct are observed at 480, 433, and 410 nm. In this case, the bathochromic effect is well reproduced in our computations. For instance, the B3 functionals give transitions at approximately 490, 470, 450, and 400 nm ($f = 0.5847, 2.2513, 0.1660$, and 0.0770 , respectively, with B3LYP/def2-TZVP). The PBE0 functional tends to underestimate the experimental data, providing first excitations at 465 and 450 nm, for instance ($f = 1.3058$ and 1.8380 , respectively, using PBE0/LANL2DZ). As usual, M06 functionals provide results intermediate between their B3 and PBE counterparts with the first bright transition at 483 nm ($f = 0.3751$ in LANL2DZ). The bathochromic effect has also been reproduced by the CCT functionals. For instance, M06-2X/def2-TZVP exhibits an intense transition at 389 nm ($f = 3.5444$), whereas it was 370 nm for the H adduct. BP86 and M06-L functionals again underestimate the excitation energies by a large extent.

4. $R = \text{NO}_2$. In this case, the observed bathochromic effect becomes very strong. Indeed, the experimental excitations are at 518, 442, and 400 nm. The B3 functional exhibits a very small transition above 650 nm ($\lambda = 672$ nm; $f = 0.0268$ with B3LYP/def2-TZVP) followed by more intense ones at approximately 550, 485, 450, and 410 nm ($f = 0.3744, 0.6693, 0.1318$, and 0.8454 , respectively, using B3LYP and the triple- ζ polarized basis set). Whereas in previous cases B3 and PBE functionals provided close results, this is no longer the case for the NO₂ adduct. Indeed, in this case, the first slightly bright transition for the PBE functionals is computed at around


580 nm ($f = 0.0390$ with PBE0/def2-TZVP), whereas the other excitations are computed at around 440, 415, and 380 nm ($f = 0.8620, 0.1910$, and 1.0400 , respectively, with PBE0/def2-TZVP). The same trend is obtained with M06. The GGA and Meta-GGA functionals give unreliable results. For instance, bright transitions have been computed above 1000 nm (BP86). Furthermore, M06-L is not much better with an intense transition at around 850 nm. CAM-B3LYP continues to overestimate the transition energy. However, this functional has the correct trend thanks to its first bright transition at around 400 nm ($f = 0.2305$ with LANL2DZ). Finally, M06-2X has a very strange behavior with several transitions between 400 and 1200 nm with very small oscillator strengths, whereas this does not happen employing the LANL2DZ basis set.

DENSITY FUNCTIONAL DEPENDENCES

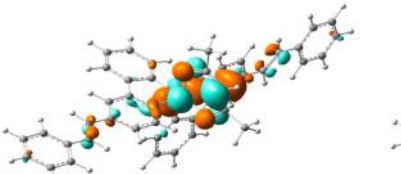
In this section, we compare the effects of the functional on Pt(II) and Ir(III) compounds (Table 1). First, one can easily discern that the BP86 and M06-L functionals are not suitable to compute TD-DFT electronic vertical transitions. Indeed, the disagreement with respect to the experimental data rises to several hundred nanometers independent of the basis set size. Turning now to hybrid functionals, it is noteworthy that the B3LYP and B3PW91 functionals provide very close and quite accurate results. For instance, in the case of iridium complexes, the differences between both functionals is <5 nm except with $R = \text{NO}_2$. With a constant shift of ~20–40 nm with respect to both Becke's functionals, PBE0 and MPW1PW91 give similar results (except, once again with $R = \text{NO}_2$).

Table 2. Selected TD-DFT Calculated Excitation Energies, Computed and Experimental Wavelengths, and Main Weights of Transitions for Ir with R = H and Pt with R = CH=C(CN)₂ (PBE0/LANL2DZ+pol) with Frontier MO plots (HOMO -2 to LUMO +2)

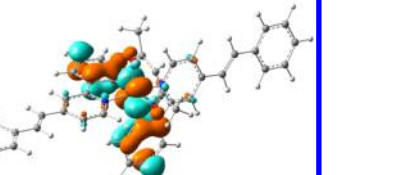
Complex	Exp (nm) [Ref. 50]	Excited States (λ_{calc} (nm)) (PBE1PBE/LANL2DZ+pol.)	Transitions (%weight)
Ir, R = H	468	S ₀ → S ₁ (486)	HOMO → LUMO +1 (96)
	410	S ₀ → S ₃ (422)	HOMO -1 → LUMO (95)
	370	S ₀ → S ₅ (385)	HOMO -2 → LUMO +1 (90)
		S ₀ → S ₇ (363)	HOMO → LUMO +2 (94)




HOMO -2




HOMO -1



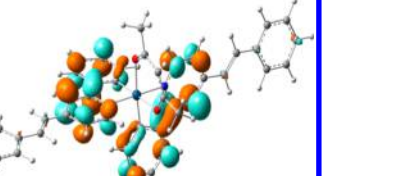
HOMO



LUMO

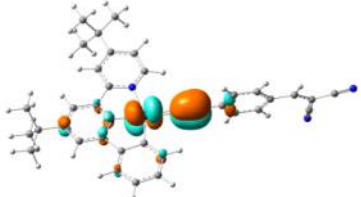


LUMO +1

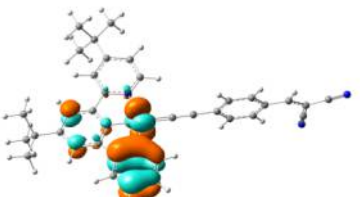


LUMO +2

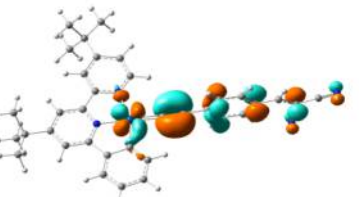
Complex	Exp (nm) [Ref. 46]	Excited States (λ_{calc} (nm)) (PBE1PBE/LANL2DZ+pol.)	Transitions (%weight)
Pt, R = CH=C(CN)₂	450	S ₀ → S ₁ (450)	HOMO -2 → LUMO (69)
			HOMO → LUMO (25)
		S ₀ → S ₂ (445)	HOMO -2 → LUMO (25)
			HOMO → LUMO (70)
	400	S ₀ → S ₅ (410)	HOMO → LUMO +1 (94)
		S ₀ → S ₆ (381)	HOMO -2 → LUMO +1 (89)
	330	S ₀ → S ₁₂ (331)	HOMO -2 → LUMO +2 (83)



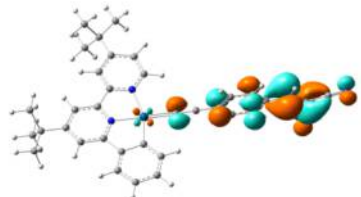
HOMO -2



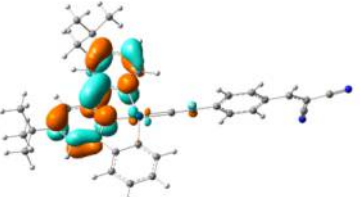
HOMO -1



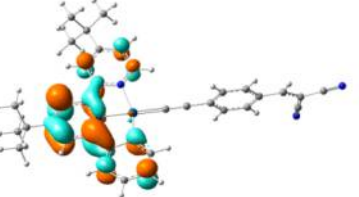
HOMO



LUMO



LUMO +1



LUMO +2

We also wish to point out that the comparable behavior of PBE0 and MPW1PW91 can be traced back to the minor differences between the functionals, where MPW1PW91 just includes some additional parameters not present in PBE0. One should also notice that the transition energies computed using the M06 functional are often intermediate between those issuing from B3 and PBE models (see the Supporting Information).

This trend of hybrid functionals has been already reported by Green and Holland in 2010. More specifically, they pointed out that careful choice of the functional with a correct amount of HF exchange can provide accurate predictions of electronic absorption spectra when one deals with metal complexes.⁷⁶ Our investigation fully confirms that the use of 20–30% of HF exchange provides, in most cases, accurate results. Moreover, as one can see in Table 1, it is difficult to unambiguously assign

specific computed excitations to their experimental counterparts for such types of compounds.

Finally, the most recent functionals involving either a high amount of HF exchange (M06-2X) or long-range corrections (CAM-B3LYP) overestimate the transitional energies forecast by more conventional hybrid functionals by an amount in some cases reaching 0.5 eV.

As a general trend, one can say that the computed vertical excitation energies for these transition metal complexes are better described by far using a global hybrid functional than a range separated hybrid one. Indeed, CAM-B3LYP has a net trend to overestimate the vertical excitation energies with respect to the experimental values. We also investigated the type of transitions for the Ir–H complex as a test case. For all reported experimental absorption bands, it turns out that, according to the computed values together with orbital plots, they mainly correspond to MLCT transitions together with LLCT (PBE0/LANL2DZ+pol) (Table 2).

■ BASIS SET AND VIBRONIC EFFECTS

As already mentioned, extending the basis set generally has a negligible effect on the vertical excitation energies. In particular, in compounds with light substituents (H, OMe), the basis set has almost no effect, whereas for the heavy substituents, there is only a slight effect. Computations using the ma-TZVP basis set did not improve the results.⁷⁷ Furthermore, the B3PW91 and PBE functionals are less affected by the basis set than M06. In Figure 1 are reported experimental and computed spectra

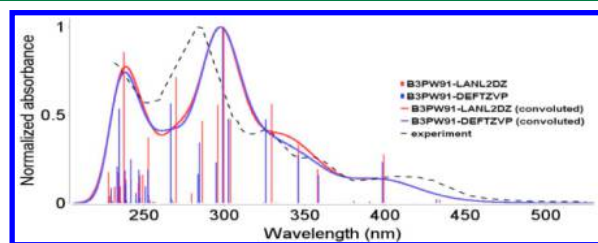


Figure 1. Normalized experimental vs computed (B3PW91/LANL2DZ+pol/def2-TZVP) absorption spectra of the Pt (R = Py) complex.

(B3PW91) of the Pt–Py compound with both basis sets. It is quite apparent that the band shape is nicely reproduced by both computations and, as mentioned before, the impact of the basis set on the transition energies is negligible, and, on the intensities, it is almost imperceptible after convolution. It should be noticed that both excitation wavelengths and intensities are well reproduced in our simulations. To be more specific, two intense peaks around 250 and 300 nm are present in the observed spectrum and nicely reproduced in our simulations. The computed vertical transition energies at 330 and 360 nm fit remarkably well to both recorded absorption peaks. A moderate peak appears at 420 nm and can be tentatively assigned to the computed excitation around 400 nm. Finally, some additional bands are present in the absorption spectrum above 450 nm. In this case, the corresponding computed transition appears around 430 nm and is very weak in intensity.

We have computed vibronic contributions at the harmonic level employing the vertical gradient approximation to further improve the simulated spectrum.⁷⁵ To this end, we computed the gradients of the first 19 excited states at the ground state

optimized geometry on the same complex as in Figure 1 at the B3PW91/LANL2DZ+pol level of theory, focusing on the 275–525 nm range.

It is clear from Figure 2 that the inclusion of vibronic couplings, even at this simple level, improves the simulated

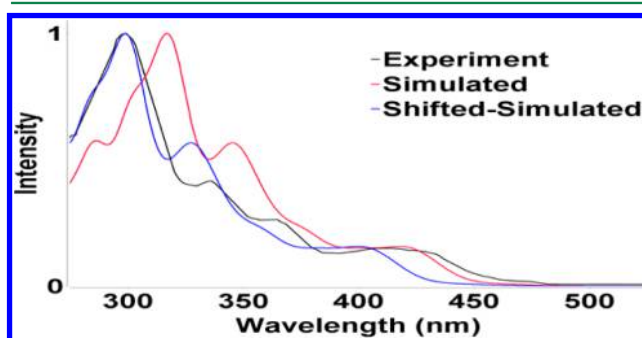


Figure 2. Experimental (black) and simulated (red; blue-shifted on the maximum) absorption spectra of the Pt (R = Py) complex (B3PW91/LANL2DZ+pol).

spectrum. Indeed, in the pure electronic spectrum (Figure 1), there were only three bands, whereas several are present in Figure 2. The intense band at 300 nm now exhibits a shoulder near the maximum. Moreover, the decrease of the peak intensity between 330 and 425 nm is nicely reproduced. In addition, the long experimental plateau around 425 nm is perfectly reproduced together with the small rise in intensity.

Concerning the global band shape, despite a slight overestimation of the peak intensity at ~350 nm, all other bands almost perfectly match their experimental counterparts. However, despite the quantitative improvements, vibronic effects do not modify the general trends discussed above, such that their computation becomes important only when quantitative accuracy is sought.

■ CONCLUSIONS

Herein, we have provided new insights about the crucial role of the choice of the most suitable density functional when one wants to investigate vertical electronic transitions of transition metal complexes. Three medium-sized backbones with Pt(II) or Ir(III) metals, already studied experimentally or theoretically, have been targeted to perform this benchmark dedicated to specialists and nonspecialists of DFT and TD-DFT computations. In each case, different terminal substituents have been used to analyze the effect of the push or pull effects. It turns out that when the terminal moiety is a push moiety or hydrogen atom, TD-DFT computations perform a good job of providing accurate yet non-prohibitively expensive vertical electronic transitions, especially when one uses classical hybrid functionals. More recent functionals (with either very high percentages of global HF exchange or with full long-range HF correction) tend to overestimate the transition energies, whereas conventional functionals (BP86/M06-L) go in the opposite direction. However, the cases of pyridine and NO₂ are more complicated, and TD-DFT faces severe difficulties in obtaining accurate transitions. We have also shown that polarized double- ζ basis sets are sufficient to obtain quite accurate results and that extension to a polarized triple- ζ level does not significantly improve the results while it dramatically increases the computational costs. Finally, in the case of iridium, the assignment of the excitations could not be made

with certainty, especially due to the lack of accuracy from the experimental data. This study has required a very large number of computations and time, but extends to one-photon absorption spectra the conclusion reached in a previous study on vibrational spectra about the importance of the choice of the functional for transition metal complexes.⁷⁸ On these grounds, we are quite confident about the feasibility of combining vibrational and electronic contributions to reach a quantitative agreement for the absorption and emission (fluorescence, phosphorescence) spectra using the tools recently developed for including vibronic contributions. It is remarkable that our previous study devoted to harmonic and anharmonic contributions to the vibrational signatures of several organometallics pointed out the key role of the correlation functional, whereas the present TD-DFT study of electronic spectra has shown that the quality of the results is mainly governed by the exchange functional.

■ ASSOCIATED CONTENT

■ Supporting Information

Excitation energies of the 25 first computed transitions for all compounds, functionals, and basis sets. The Supporting Information is available free of charge on the ACS Publications website at DOI: 10.1021/acs.jctc.5b00257.

■ AUTHOR INFORMATION

Corresponding Author

*E-mail: vincenzo.barone@sns.it.

Notes

The authors declare no competing financial interest.

■ ACKNOWLEDGMENTS

The research leading to these results has received funding from the European Union's Seventh Framework Programme (FP7/2007-2013) under Grant ERC-2012-AdG-320951-DREAMS. The authors gratefully thank the high-performance computer facilities of the DREAMS center (<http://dreamshpc.sns.it>) for providing computer resources. The support of the COST CMTS-Action CM1002 "Convergent Distributed Environment for Computational Spectroscopy (CODECS)" is also acknowledged.

■ REFERENCES

- (1) Guido, C. A.; Jacquemin, D.; Adamo, C.; Mennucci, B. On the TD-DFT Accuracy in Determining Single and Double Bonds in Excited-State Structures of Organic Molecules. *J. Phys. Chem. A* **2010**, *114*, 13402–13410.
- (2) Adamo, C.; Jacquemin, D. The Calculations of Excited-State Properties with Time-Dependent Density Functional Theory. *Chem. Soc. Rev.* **2013**, *42*, 845–856.
- (3) Chibani, S.; Le Guennic, B.; Charaf-Eddin, A.; Laurent, A. D.; Jacquemin, D. Revisiting the Optical Signatures of BODIPY with Ab Initio Tools. *Chem. Sci.* **2013**, *4*, 1950.
- (4) Laurent, A.; Jacquemin, D. Analyzing Excited-State Processes and Optical Signatures of a Ratiometric Fluorine Anion Sensor: A Quantum Look. *Sci. China: Chem.* **2014**, *57*, 1363–1368.
- (5) Boulanger, P.; Chibani, S.; Le Guennic, B.; Duchemin, I.; Blase, X.; Jacquemin, D. Combining the Bethe–Salpeter Formalism with Time-Dependent DFT Excited-State Forces to Describe Optical Signatures: NBO Fluoroborates as Working Examples. *J. Chem. Theory Comput.* **2014**, *10*, 4548–4556.
- (6) Chibani, S.; Laurent, A. D.; Blondel, A.; Mennucci, B.; Jacquemin, D. Excited-State Geometries of Solvated Molecules: Going Beyond the Linear-Response Polarizable Continuum Model. *J. Chem. Theory Comput.* **2014**, *10*, 1848–1851.
- (7) Riffet, V.; Jacquemin, D.; Cauët, E.; Frison, G. Benchmarking DFT and TD-DFT Functionals for the Ground and Excited States of Hydrogen-Rich Peptide Radicals. *J. Chem. Theory Comput.* **2014**, *10*, 3308–3318.
- (8) Laurent, A. D.; Adamo, C.; Jacquemin, D. Dye Chemistry with Time-Dependent Density Functional Theory. *Phys. Chem. Chem. Phys.* **2014**, *16*, 14334–14356.
- (9) Liang, W.; Fischer, S. A.; Frisch, M. J.; Li, X. Energy-Specific Linear Response TDHF/TDDFT for Calculating High-Energy Excited States. *J. Chem. Theory Comput.* **2011**, *7*, 3540–3547.
- (10) Jacquemin, D.; Perpète, E. A.; Ciofini, I.; Adamo, C.; Valero, R.; Zhao, Y.; Truhlar, D. G. On the Performances of the M06 Family of Density Functionals for Electronic Excitation Energies. *J. Chem. Theory Comput.* **2010**, *6*, 2071–2085.
- (11) Li, R.; Zheng, J.; Truhlar, D. G. Density Functional Approximations for Charge Transfer Excitations with Intermediate Spatial Overlap. *Phys. Chem. Chem. Phys.* **2010**, *12*, 12697–12701.
- (12) Jacquemin, D.; Zhao, Y.; Valero, R.; Adamo, C.; Ciofini, I.; Truhlar, D. G. Verdict: Time-Dependent Density Functional Theory "Not Guilty" of Large Errors for Cyanines. *J. Chem. Theory Comput.* **2012**, *8*, 1255–1259.
- (13) Isegawa, M.; Truhlar, D. G. Valence Excitation Energies of Alkenes, Carbonyl Compounds, and Azabenzenes by Time-Dependent Density Functional Theory: Linear Response of the Ground State Compared to Collinear and Noncollinear Spin-Flip TDDFT with the Tamm-Dancoff Approximation. *J. Chem. Phys.* **2013**, *138*, 134111.
- (14) Caricato, M.; Trucks, G. W.; Frisch, M. J.; Wiberg, K. B. Electronic Transition Energies: A Study of the Performance of a Large Range of Single Reference Density Functional and Wave Function Methods on Valence and Rydberg States Compared to Experiment. *J. Chem. Theory Comput.* **2010**, *6*, 370–383.
- (15) Adamo, C.; Barone, V. Inexpensive and Accurate Predictions of Optical Excitations in Transition-Metal Complexes: The TDDFT/PBE0 Route. *Theor. Chem. Acc.* **2000**, *105*, 169–172.
- (16) Angelis, F. De; Belpassi, L.; Fantacci, S. Spectroscopic Properties of Cyclometallated Iridium Complexes by TDDFT. *J. Mol. Struct.: THEOCHEM* **2009**, *914*, 74–86.
- (17) Eilmes, A. A DFT/TDDFT Study on Spectral Effects of Metal Ion Interactions with Benzofurazan-Based Fluorescent Probes. *Spectrochim. Acta, Part A* **2012**, *98*, 27–34.
- (18) Ricciardi, G.; Rosa, A.; Baerends, E. J.; van Gisbergen, S. A. J. Electronic Structure, Chemical Bond, and Optical Spectra of Metal Bis(porphyrin) Complexes: A DFT/TDDFT Study of the Bis-(porphyrin)M(IV) (M = Zr, Ce, Th) Series. *J. Am. Chem. Soc.* **2002**, *124*, 12319–12334.
- (19) Rosa, A.; Ricciardi, G.; Gritsenko, O.; Baerends, E. Excitation Energies of Metal Complexes with Time-Dependent Density Functional Theory. In *Principles and Applications of Density Functional Theory in Inorganic Chemistry I SE-2; Structure and Bonding*; Springer: Berlin, Heidelberg, 2004; Vol. 112, pp 49–116.
- (20) Steffen, A.; Costuas, K.; Boucekkine, A.; Thibault, M.-H.; Beeby, A.; Batsanov, A. S.; Charaf-Eddin, A.; Jacquemin, D.; Halet, J.-F.; Marder, T. B. Fluorescence in Rhoda- and Iridacyclopentadienes Neglecting the Spin–Orbit Coupling of the Heavy Atom: The Ligand Dominates. *Inorg. Chem.* **2014**, *53*, 7055–7069.
- (21) Latouche, C.; Lin, Y.-R.; Tobon, Y.; Furet, E.; Saillard, J.-Y.; Liu, C.-W.; Boucekkine, A. Au–Au Chemical Bonding Induced by UV Irradiation of Dinuclear Gold(i) Complexes: A Computational Study with Experimental Evidence. *Phys. Chem. Chem. Phys.* **2014**, *16*, 25840–25845.
- (22) Sahnoun, H.; Baranová, Z.; Bhuvanesh, N.; Gladysz, J. A.; Halet, J.-F. A Metal-Capped Conjugated Polyene Threaded through a Phenanthroline-Based Macrocyclic. Probing beyond the Mechanical Bond to Interactions in Interlocked Molecular Architectures. *Organometallics* **2013**, *32*, 6360–6367.
- (23) Green, K.; Gauthier, N.; Sahnoun, H.; Halet, J.-F.; Paul, F.; Fabre, B. Covalent Immobilization of Redox-Active Fe(κ^2 -dppe)(η^5 -

CSMe₅)-Based Π -Conjugated Wires on Oxide-Free Hydrogen-Terminated Silicon Surfaces. *Organometallics* **2013**, *32*, 5333–5342.

(24) Makhoul, R.; Kumamoto, Y.; Miyazaki, A.; Justaud, F.; Gendron, F.; Halet, J.-F.; Hamon, J.-R.; Lapinte, C. Synthesis and Properties of a Mixed-Valence Compound with Single-Step Tunneling and Multiple-Step Hopping Behavior. *Eur. J. Inorg. Chem.* **2014**, *2014*, 3899–3911.

(25) Latouche, C.; Lee, Y.-C.; Liao, J.-H.; Furet, E.; Saillard, J.-Y.; Liu, C. W.; Boucekkine, A. Structure and Spectroscopic Properties of Gold(I) Diselenophosph(in)ate Complexes: A Joint Experimental and Theoretical Study. *Inorg. Chem.* **2012**, *51*, 11851–11859.

(26) Baccouche, A.; Peigné, B.; Ibersiene, F.; Hammoutène, D.; Boutarfaia, A.; Boucekkine, A.; Feuvrie, C.; Maury, O.; Ledoux, L.; Le Bozec, H. Effects of the Metal Center and Substituting Groups on the Linear and Nonlinear Optical Properties of Substituted Styryl-Bipyridine Metal(II) Dichloride Complexes: DFT and TDDFT Computational Investigations and Harmonic Light Scattering Measurements. *J. Phys. Chem. A* **2010**, *114*, 5429–5438.

(27) Muniz-Miranda, F.; Menziani, M. C.; Pedone, A. DFT and TD-DFT Assessment of the Structural and Optoelectronic Properties of an Organic–Ag₁₄ Nanocluster. *J. Phys. Chem. A* **2015**, *119*, 5088–5098.

(28) Muniz-Miranda, F.; Menziani, M. C.; Pedone, A. On the Optoelectronic Properties of Phosphine and Thiolate-Protected Undeca-gold Nanoclusters. *Phys. Chem. Chem. Phys.* **2014**, *16*, 18749–18758.

(29) Liu, C. W.; Lin, Y.-R.; Fang, C.-S.; Latouche, C.; Kahlal, S.; Saillard, J.-Y. [Ag₇(H){E₂P(OR)₂}]₆ (E = Se, S): Precursors for the Fabrication of Silver Nanoparticles. *Inorg. Chem.* **2013**, *52*, 2070–2077.

(30) Liao, J.-H.; Latouche, C.; Li, B.; Kahlal, S.; Saillard, J.-Y.; Liu, C. W. A Twelve-Coordinated Iodide in a Cuboctahedral Silver(I) Skeleton. *Inorg. Chem.* **2014**, *53*, 2260–2267.

(31) Petit, L.; Maldivi, P.; Adamo, C. Predictions of Optical Excitations in Transition-Metal Complexes with Time Dependent-Density Functional Theory: Influence of Basis Sets. *J. Chem. Theory Comput.* **2005**, *1*, 953–962.

(32) Konezny, S. J.; Doherty, M. D.; Luca, O. R.; Crabtree, R. H.; Soloveichik, G. L.; Batista, V. S. Reduction of Systematic Uncertainty in DFT Redox Potentials of Transition-Metal Complexes. *J. Phys. Chem. C* **2012**, *116*, 6349–6356.

(33) Janthon, P.; Luo, S.; Kozlov, S. M.; Viñes, F.; Limtrakul, J.; Truhlar, D. G.; Illas, F. Bulk Properties of Transition Metals: A Challenge for the Design of Universal Density Functionals. *J. Chem. Theory Comput.* **2014**, *10*, 3832–3839.

(34) Jesser, A.; Rohrmüller, M.; Schmidt, W. G.; Herres-Pawlis, S. Geometrical and Optical Benchmarking of Copper Guanidine–quinoline Complexes: Insights from TD-DFT and Many-Body Perturbation Theory. *J. Comput. Chem.* **2014**, *35*, 1–17.

(35) Weymuth, T.; Couzijn, E. P. A.; Chen, P.; Reiher, M. New Benchmark Set of Transition-Metal Coordination Reactions for the Assessment of Density Functionals. *J. Chem. Theory Comput.* **2014**, *10*, 3092–3103.

(36) Boixel, J.; Guerchais, V.; Le Bozec, H.; Jacquemin, D.; Amar, A.; Boucekkine, A.; Colombo, A.; Dragonetti, C.; Marinotto, D.; Roberto, D.; Righetto, S.; De Angelis, R. Second-Order NLO Switches from Molecules to Polymer Films Based on Photochromic Cyclometalated Platinum(II) Complexes. *J. Am. Chem. Soc.* **2014**, *136*, 5367–5375.

(37) Prokhorov, A. M.; Hofbeck, T.; Czerwieniec, R.; Suleymanova, A. F.; Kozhevnikov, D. N.; Yersin, H. Brightly Luminescent Pt(II) Pincer Complexes with a Sterically Demanding Carboranyl-Phenylpyridine Ligand: A New Material Class for Diverse Optoelectronic Applications. *J. Am. Chem. Soc.* **2014**, *136*, 9637–9642.

(38) Amar, A.; Meghezzi, H.; Boixel, J.; Le Bozec, H.; Guerchais, V.; Jacquemin, D.; Boucekkine, A. Aggregation Effect on the Luminescence Properties of Phenylbipyridine Pt(II) Acetylides Complexes. A Theoretical Prediction with Experimental Evidence. *J. Phys. Chem. A* **2014**, *118*, 6278–6286.

(39) Munoz-Rodriguez, R.; Bunuel, E.; Fuentes, N.; Williams, J. A. G.; Cardenas, D. J. A Heterotrimetallic Ir(III), Au(III) and Pt(II) Complex Incorporating Cyclometalating Bi- and Tridentate Ligands: Simultaneous Emission from Different Luminescent Metal Centres

Leads to Broad-Band Light Emission. *Dalton Trans.* **2015**, *44*, 8394–8405.

(40) Septiadi, D.; Aliprandi, A.; Mauro, M.; De Cola, L. Bio-Imaging with Neutral Luminescent Pt(II) Complexes Showing Metalmetal Interactions. *RSC Adv.* **2014**, *4*, 25709–25718.

(41) Zhang, Y.; Clavadetscher, J.; Bachmann, M.; Blacque, O.; Venkatesan, K. Tuning the Luminescent Properties of Pt(II) Acetylides Complexes through Varying the Electronic Properties of N-Heterocyclic Carbene Ligands. *Inorg. Chem.* **2014**, *53*, 756–771.

(42) Kuwabara, J.; Namekawa, T.; Haga, M.; Kanbara, T. Luminescent Ir(III) Complexes Containing Benzothiazole-Based Tridentate Ligands: Synthesis, Characterization, and Application to Organic Light-Emitting Diodes. *Dalton Trans.* **2012**, *41*, 44–46.

(43) Brulatti, P.; Gildea, R. J.; Howard, J. A. K.; Fattori, V.; Cocchi, M.; Williams, J. A. G. Luminescent Iridium(III) Complexes with N⁴C⁴N-Coordinated Terdentate Ligands: Dual Tuning of the Emission Energy and Application to Organic Light-Emitting Devices. *Inorg. Chem.* **2012**, *51*, 3813–3826.

(44) Ladouceur, S.; Swanick, K. N.; Gallagher-Duval, S.; Ding, Z.; Zysman-Colman, E. Strongly Blue Luminescent Cationic Iridium(III) Complexes with an Electron-Rich Ancillary Ligand: Evaluation of Their Optoelectronic and Electrochemiluminescence Properties. *Eur. J. Inorg. Chem.* **2013**, *2013*, 5329–5343.

(45) Zaarour, M.; Singh, A.; Latouche, C.; Williams, J. A. G.; Ledoux-Rak, I.; Zyss, J.; Boucekkine, A.; Le Bozec, H.; Guerchais, V.; Dragonetti, C.; Colombo, A.; Roberto, D.; Valore, A. Linear and Nonlinear Optical Properties of Tris-Cyclometalated Phenylpyridine Ir(III) Complexes Incorporating Π -Conjugated Substituents. *Inorg. Chem.* **2013**, *52*, 7987–7994.

(46) Fillaut, J.; Akdas-Kilig, H.; Dean, E.; Latouche, C.; Boucekkine, A. Switching of Reverse Charge Transfers for a Rational Design of an OFF–ON Phosphorescent Chemodosimeter of Cyanide Anions. *Inorg. Chem.* **2013**, *52*, 4890–4897.

(47) Latouche, C.; Lanoë, P.-H.; Williams, J. A. G.; Guerchais, V.; Boucekkine, A.; Fillaut, J.-L. Switching of Excited States in Cyclometalated Platinum Complexes Incorporating Pyridyl-Acetylides Ligands (Pt–CC–py): A Combined Experimental and Theoretical Study. *New J. Chem.* **2011**, *35*, 2196–2202.

(48) Dragonetti, C.; Colombo, A.; Marinotto, D.; Righetto, S.; Roberto, D.; Valore, A.; Escadeillas, M.; Guerchais, V.; Le Bozec, H.; Boucekkine, A.; Latouche, C. Functionalized Styryl Iridium(III) Complexes as Active Second-Order NLO Chromophores and Building Blocks for SHG Polymeric Films. *J. Organomet. Chem.* **2014**, *751*, 568–572.

(49) Colombo, A.; Dragonetti, C.; Marinotto, D.; Righetto, S.; Roberto, D.; Tavazzi, S.; Escadeillas, M.; Guerchais, V.; Le Bozec, H.; Boucekkine, A.; Latouche, C. Cyclometalated 4-Styryl-2-Phenylpyridine Platinum(II) Acetylacetonate Complexes as Second-Order NLO Building Blocks for SHG Active Polymeric Films. *Organometallics* **2013**, *32*, 3890–3894.

(50) Lepeltier, M.; Lee, T. K.-M.; Lo, K. K.-W.; Toupet, L.; Le Bozec, H.; Guerchais, V. Synthesis and Photophysical Properties of Bis-Cyclometalated Iridium(III)–Styryl Complexes and Their Saturated Analogues. *Eur. J. Inorg. Chem.* **2007**, *2007*, 2734–2747.

(51) Yin, B.; Niemeyer, F.; Williams, J. A. G.; Jiang, J.; Boucekkine, A.; Toupet, L.; Le Bozec, H.; Guerchais, V. Synthesis, Structure, and Photophysical Properties of Luminescent Platinum(II) Complexes Containing Cyclometalated 4-Styryl-Functionalized 2-Phenylpyridine Ligands. *Inorg. Chem.* **2006**, *45*, 8584–8596.

(52) Frisch, M. J.; Trucks, G. W.; Schlegel, H. B.; Scuseria, G. E.; Robb, M. A.; Cheeseman, J. R.; Scalmani, G.; Barone, V.; Mennucci, B.; Petersson, G. A.; Nakatsuji, H.; Caricato, M.; Li, X.; Hratchian, H. R.; Izmaylov, A. F.; Bloino, J.; Zheng, G.; Sonnenberg, J. L.; Hada, M.; Ehara, M.; Toyota, K.; Fukuda, R.; Hasegawa, J.; Ishida, M.; Nakajima, T.; Honda, Y.; Kitao, O.; Nakai, H.; Vreven, T.; Montgomery, J. A., Jr.; Peralta, J. R.; Ogliaro, F.; Bearpark, M.; Heyd, J. J.; Brothers, E.; Kudin, K. N.; Staroverov, V. N.; Kobayashi, R.; Normand, J.; Raghavachari, K.; Rendell, A.; Burant, J. C.; Iyengar, S. S.; Tomasi, J.; Cossi, M.; Rega, N.; Millam, J. M.; Klene, M.; Knox, J. E.; Cross, J. B.; Bakken, V.;

- Adamo, C.; Jaramillo, J.; Gomperts, R.; Stratmann, R. E.; Yazyev, O.; Austin, A. J.; Cammi, R.; Pomelli, C.; Ochterski, J. W.; Martin, R. L.; Morokuma, K.; Zakrzewski, V. G.; Voth, G. A.; Salvador, P.; Dannenberg, J. J.; Dapprich, S.; Daniels, A. D.; Farkas, O.; Foresman, J. B.; Ortiz, J. V.; Cioslowski, J.; Fox, D. J. *Gaussian09*, 2013; GDVH32.
- (53) Licari, D.; Baiardi, A.; Biczysko, M.; Egidi, F.; Latouche, C.; Barone, V. Implementation of a Graphical User Interface for the Virtual Multifrequency Spectrometer: The VMS-Draw Tool. *J. Comput. Chem.* **2015**, *36*, 321–334.
- (54) Becke, A. D. Density-Functional Exchange-Energy Approximation with Correct Asymptotic Behavior. *Phys. Rev. A* **1988**, *38*, 3098–3100.
- (55) Perdew, J. P. Density-Functional Approximation for the Correlation Energy of the Inhomogeneous Electron Gas. *Phys. Rev. B* **1986**, *33*, 8822–8824.
- (56) Zhao, Y.; Truhlar, D. G. A New Local Density Functional for Main-Group Thermochemistry, Transition Metal Bonding, Thermochemical Kinetics, and Noncovalent Interactions. *J. Chem. Phys.* **2006**, *125* (194101), 1–18.
- (57) Becke, A. D. Density-Functional Thermochemistry. III. The Role of Exact Exchange. *J. Chem. Phys.* **1993**, *98*, 5648–5652.
- (58) Lee, C.; Yang, W.; Parr, R. G. Development of the Colle-Salvetti Correlation-Energy Formula into a Functional of the Electron Density. *Phys. Rev. B* **1988**, *37*, 785–789.
- (59) Stephens, P. J.; Devlin, F. J.; Chabalowski, C. F.; Frisch, M. J. Ab Initio Calculation of Vibrational Absorption and Circular Dichroism Spectra Using Density Functional Force Fields. *J. Phys. Chem.* **1994**, *98*, 11623–11627.
- (60) Perdew, J. P.; Burke, K.; Wang, Y. Generalized Gradient Approximation for the Exchange-Correlation Hole of a Many-Electron System. *Phys. Rev. B* **1996**, *54*, 16533–16539.
- (61) Perdew, J. P.; Burke, K.; Ernzerhof, M. Generalized Gradient Approximation Made Simple. *Phys. Rev. Lett.* **1996**, *77*, 3865–3868.
- (62) Adamo, C.; Barone, V. Exchange Functionals with Improved Long-Range Behavior and Adiabatic Connection Methods without Adjustable Parameters: The mPW and mPW1PW Models. *J. Chem. Phys.* **1998**, *108*, 664–675.
- (63) Adamo, C.; Barone, V. Toward Reliable Density Functional Methods without Adjustable Parameters: The PBE0Model. *J. Chem. Phys.* **1999**, *110*, 6158–6169.
- (64) Ernzerhof, M.; Scuseria, G. E. Assessment of the Perdew–Burke–Ernzerhof Exchange-Correlation Functional. *J. Chem. Phys.* **1999**, *110*, 5029–5036.
- (65) Zhao, Y.; Truhlar, D. The M06 Suite of Density Functionals for Main Group Thermochemistry, Thermochemical Kinetics, Noncovalent Interactions, Excited States, and Transition Elements: Two New Functionals and Systematic Testing of Four M06-Class Functionals and 12 Other Function. *Theor. Chem. Acc.* **2008**, *120*, 215–241.
- (66) Yanai, T.; Tew, D. P.; Handy, N. C. A New Hybrid Exchange–correlation Functional Using the Coulomb-Attenuating Method (CAM-B3LYP). *Chem. Phys. Lett.* **2004**, *393*, 51–57.
- (67) Dunning, T. H., Jr.; Hay, P. J. Gaussian Basis Sets for Molecular Calculations. In *Methods of Electronic Structure Theory SE-1*; Schaefer III, H., Ed.; Modern Theoretical Chemistry; Springer: US, 1977; Vol. 3, pp 1–27.
- (68) Hay, P. J.; Wadt, W. R. Ab Initio Effective Core Potentials for Molecular Calculations. Potentials for the Transition Metal Atoms Sc to Hg. *J. Chem. Phys.* **1985**, *82*, 270–283.
- (69) Hay, P. J.; Wadt, W. R. Ab Initio Effective Core Potentials for Molecular Calculations. Potentials for K to Au Including the Outermost Core Orbitals. *J. Chem. Phys.* **1985**, *82*, 299–310.
- (70) Wadt, W. R.; Hay, P. J. Ab Initio Effective Core Potentials for Molecular Calculations. Potentials for Main Group Elements Na to Bi. *J. Chem. Phys.* **1985**, *82*, 284–298.
- (71) Weigend, F.; Ahlrichs, R. Balanced Basis Sets of Split Valence, Triple Zeta Valence and Quadruple Zeta Valence Quality for H to Rn: Design and Assessment of Accuracy. *Phys. Chem. Chem. Phys.* **2005**, *7*, 3297–3305.
- (72) Barone, V.; Cossi, M.; Tomasi, J. A New Definition of Cavities for the Computation of Solvation Free Energies by the Polarizable Continuum Model. *J. Chem. Phys.* **1997**, *107*, 3210.
- (73) Cossi, M.; Scalmani, G.; Rega, N.; Barone, V. New Developments in the Polarizable Continuum Model for Quantum Mechanical and Classical Calculations on Molecules in Solution. *J. Chem. Phys.* **2002**, *117*, 43.
- (74) Tomasi, J.; Mennucci, B.; Cammi, R. Quantum Mechanical Continuum Solvation Models. *Chem. Rev.* **2005**, *105*, 2999–3094.
- (75) Bloino, J.; Biczysko, M.; Santoro, F.; Barone, V. General Approach to Compute Vibrationally Resolved One-Photon Electronic Spectra. *J. Chem. Theory Comput.* **2010**, *6*, 1256–1274.
- (76) Holland, J. P.; Green, J. C. Evaluation of Exchange-Correlation Functionals for Time-Dependent Density Functional Theory Calculations on Metal Complexes. *J. Comput. Chem.* **2010**, *31*, 1008–1014.
- (77) Zheng, J.; Xu, X.; Truhlar, D. Minimally Augmented Karlsruhe Basis Sets. *Theor. Chem. Acc.* **2011**, *128*, 295–305.
- (78) Latouche, C.; Palazzetti, F.; Skouteris, D.; Barone, V. High Accuracy Vibrational Computations for Transition Metal Complexes Including Anharmonic Corrections: Ferrocene, Ruthenocene and Osmocene as Test Cases. *J. Chem. Theory Comput.* **2014**, *10*, 4565–4573.